

Phase-Space Description of Momentum Spectra in Relativistic Heavy-Ion Collisions

Werner Deinet* and Dirk H. Rischke†

*Institut für Theoretische Physik, Johann Wolfgang Goethe-Universität,
Max-von-Laue-Str. 1, D-60438 Frankfurt am Main, Germany*

(Dated: May 20, 2019)

We consider a phase-space model for particle production in nuclear collisions. Once the multiplicities of the individual particle species are known, single-inclusive momentum spectra can be computed after making simplifying assumptions for the matrix element for multiparticle production. Comparison of the calculated spectra with data for pions and kaons from central Pb+Pb collisions at $E_{\text{Lab}} = 158$ AGeV reveals a residual longitudinal phase-space dominance in the final state of the reaction. We account for this by modifying the isotropic, relativistic invariant phase space in a way which retains boost invariance in beam direction but suppresses large transverse momenta. Adjusting a single parameter, we obtain a reasonably good description of transverse momentum and rapidity spectra for both pions and kaons.

I. INTRODUCTION

In relativistic heavy-ion collisions one can study strongly interacting matter under extreme conditions [1]. Of particular interest is the question whether a novel phase of nuclear matter, the so-called quark-gluon plasma (QGP), can be created in such collisions. In this phase, quarks and gluons are deconfined and chiral symmetry is restored. Lattice QCD calculations [2] predict that, in thermodynamical equilibrium, this phase occurs at temperatures above ~ 170 MeV (for vanishing baryon chemical potential). Such temperatures are expected to be reached and exceeded for collisions at CERN-SPS and BNL-RHIC energies, respectively.

In nucleus-nucleus collisions at ultrarelativistic energies, secondary particles are copiously produced over a small region in space-time. It is then natural to assume that interactions between these particles drive the system towards (local) thermodynamical equilibrium. Indeed, measured single-inclusive transverse momentum spectra of individual particle species show an exponential decrease similar to that expected in thermal equilibrium. Following this line of arguments, one has studied the evolution of the system using models based on ideal fluid dynamics where the system is assumed to be in local thermodynamical equilibrium. At RHIC energies, such models are able to reproduce the data for single-inclusive transverse momentum spectra of various particle species [3]. A particular success of the fluidynamical approach was the correct prediction of the magnitude of elliptic flow. The fact that data on elliptic flow seem to saturate the ideal fluid limit has recently led to the speculation that matter created in collisions at RHIC energies is a so-called *strongly coupled QGP* with very small viscosity over entropy ratio [4].

However, the fluidynamical approach is not without problems. A long-standing problem is the so-called “HBT puzzle”, i.e., the fact that HBT correlation radii and single-inclusive particle spectra cannot be simultaneously described within the fluidynamical approach [5].

Another problem of the fluidynamical approach concerns the reproduction of the measured particle ratios. Under the assumption of local thermodynamical equilibrium, as well as conservation of electric charge and strangeness, one can determine from such particle ratios the temperature and the baryon chemical potential of the system on the hypersurface where chemical freeze-out occurs, i.e., where inelastic collisions cease and the multiplicities of produced particles no longer change [6–8]. The values for the chemical freeze-out temperature and baryon chemical potential thus obtained indicate that the system undergoes chemical freeze-out well before thermal freeze-out, i.e., when also elastic collisions cease and the single-inclusive particle spectra no longer change their shape. If one accounts for this in the fluidynamical evolution by allowing for departures from chemical equilibrium [9] and thus keeps the particle ratios at their experimental values, one is no longer able to describe data for collective flow [10]. (An exception is the study of Ref. [11] which reproduces the transverse mass spectra *and* multiplicities for pions, kaons, and (anti-)protons for collisions at RHIC energies assuming simultaneous thermal and chemical freeze-out.)

In this paper, we pursue a different strategy of describing single-inclusive momentum spectra of particles produced in heavy-ion collisions. Our arguments are solely based on the phase space of the particles in the final state. Thus, we follow a well-known and well-documented approach in the physics of hadron-hadron collisions [12–14] and apply

*Electronic address: deinet@th.physik.uni-frankfurt.de

†Electronic address: drischke@th.physik.uni-frankfurt.de

it to nucleus-nucleus collisions [15–19]. In order to determine the phase space, we need to know the experimentally measured multiplicities of secondary particles. We also have to make simplifying assumption for the matrix element of multiparticle production. We can then determine single-inclusive particle spectra and compare them with the experimentally measured spectra.

This phase-space model to describe single-inclusive particle spectra represents an approach with the minimum number of assumptions concerning the dynamics of the reaction. In its most simple form it relies solely on the constraints imposed by the kinematics of the reaction, such as total energy and particle multiplicities. Deviations from the phase-space model are a clear indication for nontrivial dynamics beyond pure kinematics.

Our approach is complementary to the fluid-/thermodynamical approach. There, the exponential decay of transverse mass spectra as seen in the data is the motivation to argue that matter is in local thermodynamical equilibrium. On the other hand, the data deviates from this exponential decay, especially in the region of small transverse momenta. These deviations are commonly attributed to resonance decays and to collective motion. Particle ratios can be predicted, once temperature and baryon chemical potential at chemical freeze-out are known. On the other hand, in our approach particle multiplicities serve as input to determine the size of multiparticle phase space. Once they are known, single-inclusive particle spectra can be computed. As we shall see, the calculated transverse mass spectra also decay exponentially. Similar to the fluid-/thermodynamical approach we then interpret the deviation of the data from a pure exponential decay as a signature for nontrivial dynamics, such as resonance decays and collective flow of matter.

For this study, as an example we use data [20–25] of the NA49 collaboration for the 5% most central Pb+Pb collisions at a beam energy of $E_{\text{Lab}} = 158$ AGeV, corresponding to $\sqrt{s_{NN}} = 17.3$ AGeV in the center-of-momentum frame. For the 5% most central collisions, the average number of wounded nucleons is $\langle N_w \rangle = 362$. Therefore, the total energy deposited in the reaction is estimated to be $\sqrt{s} = \sqrt{s_{NN}} \frac{\langle N_w \rangle}{2} = 3131.3$ GeV. In principle, we could also have used data from other experiments, but the advantage of the NA49 experiment is that it provides full rapidity coverage. It thus allows us to investigate rapidity spectra in addition to the transverse mass spectra.

This paper is organized as follows. In Sec. II we define and compute the phase-space integral. In practice, the computation is not possible unless one makes simplifying assumptions for the matrix element for multiparticle production. We investigate a product ansatz for the matrix element, which allows to factorize the phase-space integral and thus facilitates the computation. We then study two special cases in more detail, one which is completely isotropic in phase space and preserves general Lorentz invariance, and another which incorporates the longitudinal phase-space dominance of the reaction and only preserves Lorentz invariance under boosts in beam direction. In Sec. III we compute single-inclusive momentum spectra, i.e., transverse mass and rapidity spectra, from the phase-space integral and point out differences to momentum spectra in thermal equilibrium. In Sec. IV we confront the calculated spectra with experimental data. To this end, it was also necessary to reconstruct the multiplicities of unmeasured particle species using symmetry considerations, an empirical rule, and a simple quark model. Section V concludes this work with a summary and an outlook. Our units are $\hbar = c = k_B = 1$ and the metric tensor is chosen as $g^{\mu\nu} = (+, -, -, -)$.

II. THE PHASE-SPACE INTEGRAL

Let us consider the cross section for production of secondaries in collisions of elementary particles (or nuclei). The particles (or nuclei) in the incoming channel have masses m_a , m_b and four-momenta p_a , p_b . The center-of-momentum energy (squared) of the reaction is $s \equiv P^2$, where $P^\mu = (E, \mathbf{P}) = p_a^\mu + p_b^\mu$ is the total four-momentum. We assume that there are n particles in the final state with masses m_1, \dots, m_n and four-momenta p_1^μ, \dots, p_n^μ , where $p_i^\mu = (E_i, \mathbf{p}_i)$, with $E_i = \sqrt{\mathbf{p}_i^2 + m_i^2}$. The cross section σ for this reaction is given by

$$\sigma = \frac{1}{F} I_n(P^\mu), \quad (1)$$

where

$$F \equiv 2 \sqrt{\lambda(s, m_a, m_b)} (2\pi)^{3n-4} \quad (2)$$

is the flux factor, with $\lambda(x, y, z) = x^2 + y^2 + z^2 - 2xy - 2yz - 2zx$ being the kinematical function [13]. I_n is an integral over the $3n$ -dimensional invariant momentum space of the secondaries,

$$I_n(P^\mu) = \int \prod_{i=1}^n \frac{d^3 p_i}{2E_i} \delta^4(P^\mu - \sum_j p_j^\mu) T(\mathbf{p}_i). \quad (3)$$

The integrand consists of a four-dimensional, four-momentum conserving δ -function and of the square $T(\mathbf{p}_i)$ of the transition matrix element.

The secondaries produced in a reaction come in different species r . The multiplicity of particles of species r is denoted by n_r , such that $n = \sum_r n_r$. In order to compute I_n one needs to specify the multiplicities n_r . These differ from event to event. Usually, event-averaged quantities are given in the literature. We shall exclusively use these event-averaged multiplicities in the following. We shall see that our results do not change qualitatively if we vary the multiplicities n_r within a factor of $3\sqrt{n_r}$, where we assume $\sqrt{n_r}$ to be a measure for the statistical error. One could also study multiparticle production on an event-by-event basis [26] in order to examine particle number fluctuations, but this is beyond the scope of the present work.

In order to calculate I_n , according to Eq. (3) $3n$ integrations have to be performed, where in our case n is larger than 2000. The δ^4 -function prevents that these integrals decouple. Therefore, the computation of I_n requires in general numerical methods. One can distinguish three approaches, recursion relations [12, 13, 27], Monte Carlo methods [28, 29], and the statistical approach [13]. In this work we employ the latter, because they are most appropriate for a large number of secondaries. The essential idea is to use standard methods of statistical mechanics [30–35]. In statistical mechanics, calculations performed in the microcanonical ensemble are difficult, because the energy is fixed. Therefore, one replaces the microcanonical ensemble by the canonical ensemble, where the energy can vary, but the temperature is fixed. In the thermodynamical limit, i.e., for large particle numbers, both approaches yield identical results. The same idea is applied here to compute I_n , but there exist several methods which differ in detail. Some use the central-limit theorem of probability theory, as suggested and explored by Khinchin [36]. In this work, we employ the saddle-point method [34], which yields, in the approximation used here, the same result as the methods based on the central-limit theorem.

A. The calculation of the phase-space integral

In general, for multiparticle reactions the matrix element $T(\mathbf{p}_i)$ is too complicated to calculate analytically. Therefore, in order to make progress one resorts to simple approximations for $T(\mathbf{p}_i)$. Such an approximation can be motivated by the symmetries of the problem, and it should not spoil the Lorentz invariance of I_n . Our particular ansatz used in the following is

$$T(\mathbf{p}_i) = \prod_{i=1}^n f_i(\mathbf{p}_{\perp i}) . \quad (4)$$

The most simple case, without any assumptions about the symmetries of the problem and preserving full Lorentz invariance, is

$$f_i(\mathbf{p}_{\perp i}) = 1 . \quad (5)$$

Another case studied here is motivated by the longitudinal phase-space dominance in hadron-hadron and high-energy nuclear collisions. Choosing

$$f_i(\mathbf{p}_{\perp i}) = \exp [-a(m_{\perp i} - m_i)] , \quad (6)$$

where $m_{\perp i} = \sqrt{p_{\perp i}^2 + m_i^2}$ is the transverse mass, the transverse phase space is exponentially suppressed. This ansatz preserves boost invariance with respect to the beam axis, but is no longer invariant under Lorentz transformations perpendicular to this direction.

Inserting the ansatz (4) into Eq. (3), we obtain

$$I_n(P^\mu) = \int \prod_{i=1}^n \frac{d^3 p_i}{2E_i} f_i(\mathbf{p}_{\perp i}) \delta^4(P^\mu - \sum_j p_j^\mu) . \quad (7)$$

The momentum integrals are decoupled by performing a Laplace transformation,

$$\Phi_n(\alpha_\mu) = \int d^4 P \exp (-\alpha_\nu P^\nu) I_n(P^\mu) . \quad (8)$$

The Laplace transform Φ_n is a function of the four-vector α_μ . Inserting I_n into Eq. (8) and performing the integration over P^μ , we obtain

$$\begin{aligned} \Phi_n(\alpha_\mu) &= \int d^4 P \prod_{i=1}^n \frac{d^3 p_i}{2E_i} f_i(\mathbf{p}_{\perp i}) \delta^4(P^\mu - \sum_j p_j^\mu) \exp (-\alpha_\nu P^\nu) \\ &= \int \prod_{i=1}^n \frac{d^3 p_i}{2E_i} f_i(\mathbf{p}_{\perp i}) \exp (-\alpha_\nu p_i^\nu) . \end{aligned} \quad (9)$$

We define the functions

$$\phi_i(\alpha_\mu) = \int \frac{d^3 p_i}{2E_i} f_i(\mathbf{p}_{\perp i}) \exp(-\alpha_\nu p_i^\nu) , \quad (10)$$

such that

$$\Phi_n(\alpha_\mu) = \prod_{i=1}^n \phi_i(\alpha_\mu) . \quad (11)$$

The original integral I_n can be obtained from the inverse Laplace transformation,

$$I_n(P^\mu) = \frac{1}{(2\pi i)^4} \int_{c_\mu - i\infty}^{c_\mu + i\infty} d^4 \alpha \exp(\alpha_\nu P^\nu) \Phi_n(\alpha_\mu) . \quad (12)$$

The path of integration is parallel to the imaginary axis, where c_μ is a constant 4-vector. Each component c_μ is chosen such that the path of integration lies in a range of values for α_μ , where the integrand does not have any singularities.

We proceed by taking Φ_n into the argument of the exponential function,

$$I_n(P^\mu) = \frac{1}{(2\pi i)^4} \int_{c_\mu - i\infty}^{c_\mu + i\infty} d^4 \alpha \exp[F(\alpha_\mu)] , \quad (13)$$

where we defined

$$F(\alpha_\mu) \equiv \alpha_\nu P^\nu + \ln \Phi_n(\alpha_\mu) . \quad (14)$$

In general, the integral (13) cannot be solved analytically. Statistical methods are used to obtain an approximative solution. Here, we employ the saddle-point approximation [13, 34]. The saddle point of the integrand, β_μ , is given by the condition

$$\left. \frac{\partial F(\alpha_\mu)}{\partial \alpha_\nu} \right|_{\alpha_\mu = \beta_\mu} = 0 , \quad (15)$$

or, with Eq. (14),

$$P^\nu = -\frac{\partial \ln \Phi_n(\beta_\mu)}{\partial \beta_\nu} = -\sum_{i=1}^n \frac{1}{\phi_i(\beta_\mu)} \int \frac{d^3 p_i}{2E_i} f_i(\mathbf{p}_{\perp i}) p_i^\nu \exp(-\beta_\lambda p_i^\lambda) . \quad (16)$$

Going into the rest frame of the saddle point, $\beta^\mu = (\beta, \mathbf{0})$ and using the fact that $f(\mathbf{p}_{\perp i})$ and $p_i^0 \equiv E_i$ are even functions of momentum, we observe that this rest frame is identical to the center-of-momentum frame, $P^\mu = (\sqrt{s}, \mathbf{0})$. Thus, β^μ and P^μ must be proportional to each other, $P^\mu \sim \beta^\mu$, in any frame which differs from the rest frame by a boost in longitudinal direction. We now determine the constant of proportionality. To this end, we compute the four-gradient of $\ln \Phi_n$ at the saddle point assuming Φ_n to be a function of the absolute value $\beta = \sqrt{\beta_\nu \beta^\nu}$ of β^μ , and its direction, $\hat{\beta}^\mu \equiv \beta^\mu / \beta$. Then,

$$P^\nu = -\frac{\partial \ln \Phi_n(\beta, \hat{\beta}_\mu)}{\partial \beta_\nu} = -\frac{\partial \ln \Phi_n(\beta, \hat{\beta}_\mu)}{\partial \beta} \hat{\beta}^\nu - \frac{\partial \ln \Phi_n(\beta, \hat{\beta}_\mu)}{\partial \hat{\beta}_\lambda} \frac{1}{\beta} B_\lambda^\nu , \quad (17)$$

where

$$B_\lambda^\nu \equiv \beta \frac{\partial \hat{\beta}_\lambda}{\partial \beta_\nu} = g_\lambda^\nu - \hat{\beta}_\lambda \hat{\beta}^\nu \quad (18)$$

is the projector onto the direction which is four-transverse to β^μ . However, since β^μ and P^μ are proportional to each other, the part proportional to B_λ^ν must be zero, i.e., there is no dependence of $\ln \Phi_n$ on $\hat{\beta}^\mu$, and we have

$$P^\nu = -\frac{\partial \ln \Phi_n(\beta)}{\partial \beta} \hat{\beta}^\nu . \quad (19)$$

Going to the center-of-momentum frame, this equation serves to (implicitly) determine the absolute value of β ,

$$\sqrt{s} = -\frac{\partial \ln \Phi_n(\beta)}{\partial \beta} = \frac{1}{2} \sum_{i=1}^n \frac{1}{\phi_i(\beta)} \int d^3 p_i f_i(\mathbf{p}_{\perp i}) e^{-\beta E_i}. \quad (20)$$

We now proceed with the evaluation of the integral (13). We choose the integration path to lead through the saddle point and change the integration variable to $t^\mu \equiv -i(\alpha^\mu - \beta^\mu)$. For large particle numbers the integrand is sharply peaked around the saddle point, $t^\mu = 0$, and we may employ a Taylor expansion of the function $F(\alpha_\mu)$. For our numerical calculations presented below, we checked that terms higher than second order in this expansion are at most of the order of $\sim 10^{-4}$ and thus insignificant. We therefore restrict the following consideration to terms of second order in t^μ ,

$$F(\alpha_\mu) = F(\beta_\mu) - \frac{1}{2} t^\nu t^\lambda F_{\nu\lambda} + O(t^3), \quad (21)$$

where we used the saddle-point condition (15) to eliminate the linear term in t^μ , and where the second derivative of $F(\alpha_\mu)$ with respect to α_ν at the saddle point is denoted as

$$F_{\nu\lambda} \equiv \left. \frac{\partial^2 F(\alpha_\mu)}{\partial \alpha^\nu \partial \alpha^\lambda} \right|_{\alpha_\mu = \beta_\mu}. \quad (22)$$

Using Eq. (14) and the fact that $\ln \Phi_n$ only depends on the absolute value of β^μ , we can further evaluate $F_{\nu\lambda}$,

$$F_{\nu\lambda} = \frac{\partial^2 \ln \Phi_n(\beta)}{\partial \beta^\nu \partial \beta^\lambda} = \frac{\kappa}{\beta^2} \hat{\beta}_\nu \hat{\beta}_\lambda - \frac{\sqrt{s}}{\beta} B_{\nu\lambda}, \quad (23)$$

where we employed Eqs. (18) and (20) and defined

$$\kappa \equiv \beta^2 \frac{\partial^2 \ln \Phi_n(\beta)}{\partial \beta^2} = \frac{\beta^2}{4} \sum_{i=1}^n \frac{1}{\phi_i(\beta)} \left\{ 2 \int d^3 p_i f_i(\mathbf{p}_{\perp i}) E_i e^{-\beta E_i} - \frac{1}{\phi_i(\beta)} \left[\int d^3 p_i f_i(\mathbf{p}_{\perp i}) e^{-\beta E_i} \right]^2 \right\}. \quad (24)$$

For the explicit expression on the right-hand side we have chosen the rest frame of β^μ . Inserting the Taylor expansion into Eq. (13) we obtain

$$I_n(P^\mu) \simeq \frac{e^{\beta \sqrt{s}} \Phi_n(\beta)}{(2\pi)^4} \int d^4 t \exp \left\{ -\frac{1}{2\beta^2} \left[\kappa (t^\nu \hat{\beta}_\nu)^2 - \beta \sqrt{s} t^\nu B_{\nu\lambda} t^\lambda \right] \right\}. \quad (25)$$

We evaluate the t -integral in the rest frame of β^μ , where

$$\kappa (t^\nu \hat{\beta}_\nu)^2 - \beta \sqrt{s} t^\nu B_{\nu\lambda} t^\lambda = \kappa t_0^2 + \beta \sqrt{s} \mathbf{t} \cdot \mathbf{t}, \quad (26)$$

i.e., the integral decouples into four Gaussian integrals. The final result is

$$I_n(P^\mu) \simeq \frac{e^{\beta \sqrt{s}}}{4\pi^2} \Phi_n(\beta) \frac{\beta}{\sqrt{\kappa}} \left(\frac{\beta}{\sqrt{s}} \right)^{3/2}. \quad (27)$$

For large multiplicities n , the logarithm of this expression can be estimated as

$$\ln I_n(P^\mu) \simeq \beta \sqrt{s} + \ln \Phi_n(\beta). \quad (28)$$

Here, we have only kept terms of order $O(n)$, such as \sqrt{s} . Terms proportional to $\ln \beta$ are of order $O(1)$, because β itself is $\sim O(1)$, see e.g. Eq. (34) below for the massless case. Also, terms of order $\ln \sqrt{s}$ and $\ln \kappa$ are of order $O(1)$, because \sqrt{s} and κ are of order $O(n)$, see e.g. Eq. (35) below, and thus $\ln \sqrt{s} \sim \ln \kappa \sim O(1)$. Thus, with Eq. (20) we obtain

$$\frac{\partial \ln I_n(P^\mu)}{\partial \sqrt{s}} \equiv 2\sqrt{s} \frac{\partial \ln I_n(P^\mu)}{\partial s} \simeq \beta + \frac{\partial \beta}{\partial \sqrt{s}} \left(\sqrt{s} + \frac{\ln \Phi_n(\beta)}{\partial \beta} \right) \equiv \beta. \quad (29)$$

B. Special cases

We now discuss some special cases of the result (27). In the case (5), Φ_n is invariant under any Lorentz transformation and thus can only depend on the Lorentz-scalar quantity $\beta = \sqrt{\beta^\nu \beta_\nu}$. It may be computed in any frame, but the rest frame of β^μ is particularly convenient. In this frame [37, 38],

$$\phi_i(\beta) = 2\pi \int_0^\infty dp_i \frac{p_i^2}{E_i} e^{-\beta E_i} = \frac{2\pi m_i}{\beta} K_1(\beta m_i) , \quad (30)$$

and $\Phi(\beta)$ is readily obtained from Eq. (11). The saddle-point condition (20) reads

$$\sqrt{s} = \frac{2n}{\beta} + \sum_{i=1}^n m_i \frac{K_0(\beta m_i)}{K_1(\beta m_i)} , \quad (31)$$

and κ is determined as

$$\kappa = 4n - \beta \sqrt{s} + \beta^2 \sum_i m_i^2 \left\{ 1 - \left[\frac{K_0(\beta m_i)}{K_1(\beta m_i)} \right]^2 \right\} . \quad (32)$$

If all particles are massless, we obtain

$$\phi_i(\beta) = \frac{2\pi}{\beta^2} , \quad (33)$$

where the saddle point is given by

$$\beta = \frac{2n}{\sqrt{s}} . \quad (34)$$

Finally,

$$\kappa = 4n - \beta \sqrt{s} \equiv 2n , \quad (35)$$

such that

$$I_n(P^\mu) \simeq \frac{e^{2n} \pi^{n-2}}{2^n n^2} \left(\frac{\sqrt{s}}{n} \right)^{2n-4} . \quad (36)$$

The exact result is [34]

$$I_n(P^\mu) = \frac{\pi^{n-1}}{2^{n-1} (n-1)! (n-2)!} \sqrt{s}^{2n-4} . \quad (37)$$

For large n , one may approximate the factorials with the help of Stirling's formula. Using $(1 - x/n)^n \rightarrow e^{-x}$ for $n \rightarrow \infty$, one then observes that the result (36) obtained via the saddle-point method is consistent with the exact result (37).

In the case (6), Φ_n is invariant under Lorentz transformations along the z -axis. Again, we compute it in the rest frame of β^μ . Defining the function

$$\mathcal{J}_{l,m}(x, y) \equiv 2\pi e^y \int_x^\infty dz z^l e^{-yz/x} K_m(z) , \quad (38)$$

we obtain

$$\phi_i(\beta) = \beta^{-2} \mathcal{J}_{1,0}(\beta m_i, am_i) . \quad (39)$$

The saddle-point condition (20) now reads

$$\sqrt{s} = \frac{1}{\beta} \sum_{i=1}^n \frac{\mathcal{J}_{2,1}(\beta m_i, am_i)}{\mathcal{J}_{1,0}(\beta m_i, am_i)} . \quad (40)$$

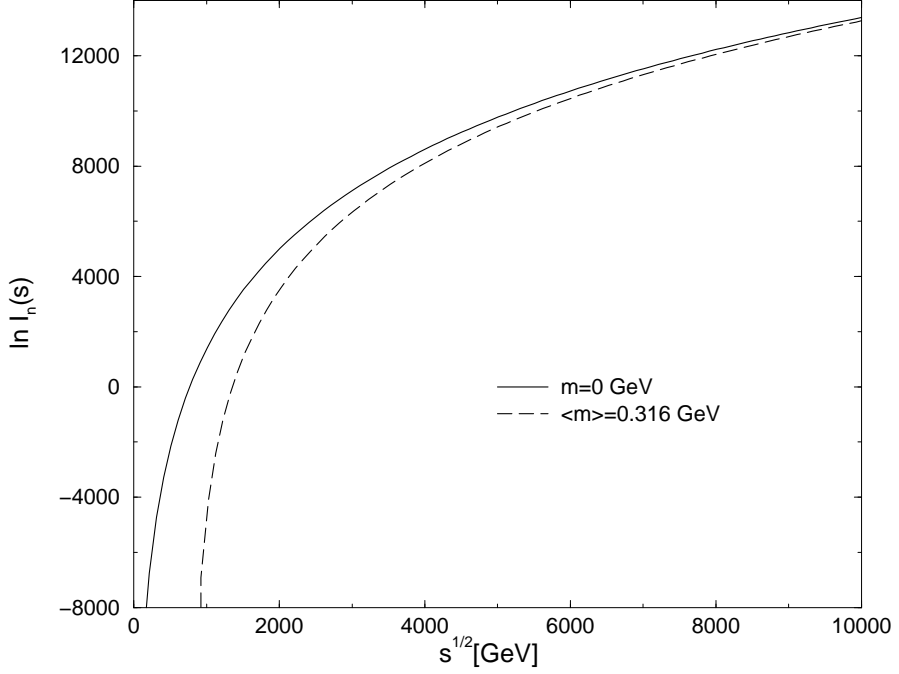


FIG. 1: The logarithm of the phase-space integral for $n = 2611$ massless particles (solid curve) and for massive particles as listed in Table II (dashed curve). Both curves are computed for $a = 0$.

The coefficient κ is determined as

$$\kappa = \sum_{i=1}^n \left\{ \frac{\mathcal{J}_{3,0}(\beta m_i, am_i) + \mathcal{J}_{2,1}(\beta m_i, am_i)}{\mathcal{J}_{1,0}(\beta m_i, am_i)} - \left[\frac{\mathcal{J}_{2,1}(\beta m_i, am_i)}{\mathcal{J}_{1,0}(\beta m_i, am_i)} \right]^2 \right\}. \quad (41)$$

In order to get a feeling for the magnitude of the phase-space integral consider the hadron multiplicities given in Table II. There are $n = 2611$ secondaries with a total rest mass of $\sum m_i = 824.65$ GeV. The average particle mass is $\langle m_i \rangle \simeq 0.316$ GeV. The total available energy is $\sqrt{s} = 3131.3$ GeV, see introduction. For $a = 0$, this results in $I_n \simeq 0.5 \cdot 10^{2867}$, or $\ln I_n \simeq 6600$. The saddle point of the t -integration is located at $\beta = 2.027 \text{ GeV}^{-1}$. In Fig. 1 we show the logarithm of the phase-space integral as a function of \sqrt{s} for 2611 massless particles and for the set of 2611 particles of Table II. For a given \sqrt{s} , the result for massive particles is always below that of massless particles, since some of the energy is used to generate the rest mass of the particles and is no longer available for the phase-space volume occupied by the system. Only when $\sqrt{s} \rightarrow \infty$, the massive case approaches the result for massless particles.

The influence of the parameter a on the value of the phase-space integral is demonstrated in Fig. 2. The phase-space integral is again computed with the set of particles listed in Table II. The value of the integral decreases with increasing a , which is naturally explained by the exponential suppression of transverse phase space, cf. Eq. (6).

III. SINGLE-INCLUSIVE PARTICLE SPECTRA

In this section we demonstrate how one can compute single-inclusive particle spectra from the phase-space integral discussed in the previous section. For comparison, we also present the calculation of single-inclusive spectra in thermal equilibrium.

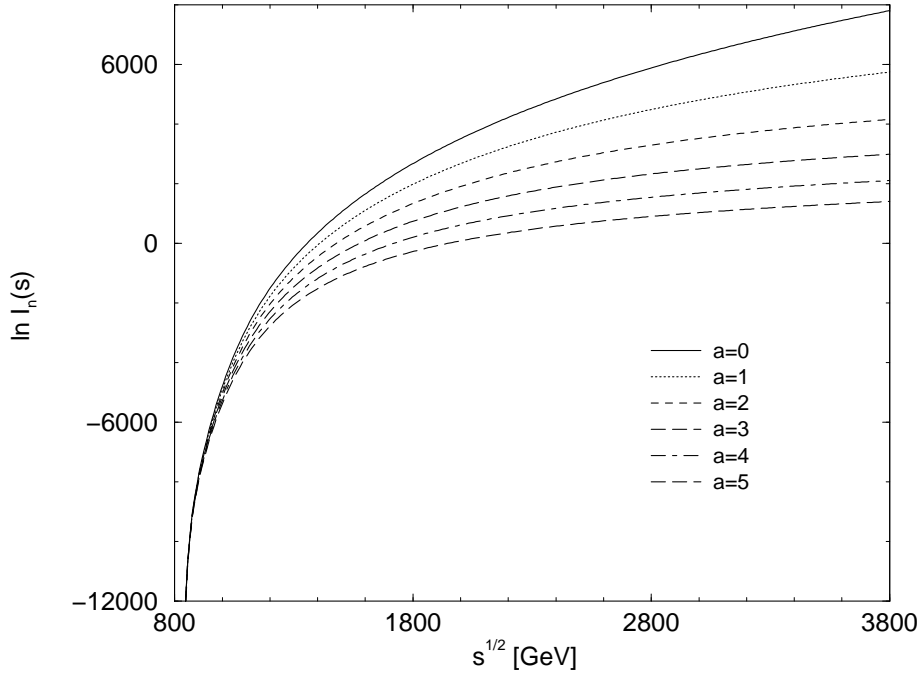


FIG. 2: The phase-space integral for particles as listed in Table II for different values of the parameter a (in units of GeV^{-1}).

A. Particle spectra from phase space

According to Eq. (1), the differential cross section for inclusive production of, say, the n th secondary particle is

$$\begin{aligned}
 E_n \frac{d^3\sigma}{d^3p_n} &= \frac{E_n}{F} \frac{d^3I_n(P^\mu)}{d^3p_n} \\
 &= \frac{f_n(\mathbf{p}_{\perp n})}{2F} \int \prod_{i=1}^{n-1} \frac{d^3p_i}{2E_i} f_i(\mathbf{p}_{\perp i}) \delta^4(P^\mu - p_n^\mu - \sum_j p_j^\mu) \\
 &= \frac{f_n(\mathbf{p}_{\perp n})}{2F} I_{n-1}(P^\mu - p_n^\mu).
 \end{aligned} \tag{42}$$

I_{n-1} is the phase-space integral for the first $n - 1$ particles at a reduced center-of-momentum frame energy,

$$s' \equiv (P - p_n)^2 = s + m_n^2 - 2E_n \sqrt{s} = s + m_n^2 - 2m_{\perp n} \cosh y_n \sqrt{s}. \tag{43}$$

The single-inclusive particle spectrum is obtained from the differential cross section (42) via

$$E_n \frac{d^3n_n}{d^3p_n} = \langle n_n \rangle \frac{E_n}{\sigma} \frac{d^3\sigma}{d^3p_n} = \langle n_n \rangle \frac{f_n(\mathbf{p}_{\perp n})}{2} \frac{I_{n-1}(P^\mu - p_n^\mu)}{I_n(P^\mu)}. \tag{44}$$

As discussed in the previous section, the calculation of the phase-space integrals on the right-hand side will be done in the rest frame of the collision. However, because there are $n - 1$ particles in the numerator and n particles in the denominator, the rest frame of I_{n-1} will be different from that of I_n . This is irrelevant if the phase-space integral is Lorentz invariant, such that $I_{n-1}(P^\mu - p_n^\mu) \equiv I_{n-1}(s')$ and $I_n(P^\mu) \equiv I_n(s)$. If the phase-space integral is only Lorentz invariant with respect to boosts along the z -axis, this difference is also irrelevant if the n th particle moves along this axis. If not, we assume the recoil in transverse direction to be sufficiently small such that the rest frame of I_{n-1} is approximately the same as that of I_n . This is certainly a good approximation for large n .

Transverse mass spectra are obtained from Eq. (44) after integrating over the transverse polar angle,

$$\frac{1}{m_{\perp n}} \frac{d^2n_n}{dm_{\perp n} dy_n} \simeq \pi \langle n_n \rangle f_n(\mathbf{p}_{\perp n}) \frac{I_{n-1}(s')}{I_n(s)}. \tag{45}$$

An additional integration over $m_{\perp n}$ yields the rapidity spectrum,

$$\frac{dn_n}{dy_n} \simeq \pi \langle n_n \rangle \int_{m_n}^{\infty} dm_{\perp n} m_{\perp n} f_n(\mathbf{p}_{\perp n}) \frac{I_{n-1}(s')}{I_n(s)} . \quad (46)$$

A further integration over y_n then gives the multiplicity of the n -th particle, which is an input parameter. This integration serves as a check for the consistency of our results.

In the following, we discuss several special cases of the general result (45) for the transverse mass spectra.

B. Special cases

Let us consider the case (6) for the function $f_i(\mathbf{p}_{\perp i})$. The other case (5) can be simply obtained by setting $a = 0$ in the final result. In Eq. (45), exponentiate the numerator $I_{n-1}(s')$ and expand $\ln I_{n-1}(s')$ to first order in $s' - (s + m_n^2) = -2m_{\perp n} \cosh y_n \sqrt{s}$ [27]. This is a good approximation, since the energy of a single particle is small compared to the total energy in the system, $E_n \equiv m_{\perp n} \cosh y_n \ll \sqrt{s}$. We may also drop m_n^2 compared to s . We obtain

$$\frac{1}{m_{\perp n}} \frac{d^2 n_n}{dm_{\perp n} dy_n} \simeq \pi \langle n_n \rangle e^{a m_n} \frac{I_{n-1}(s)}{I_n(s)} \exp\left(-\frac{m_{\perp n}}{T^*}\right) . \quad (47)$$

Here we defined the slope parameter

$$\frac{1}{T^*} \equiv 2\sqrt{s} \cosh y_n \frac{d}{ds} \ln I_{n-1}(s) + a \simeq \beta \cosh y_n + a , \quad (48)$$

where we have used Eq. (29) and the fact that $n-1 \simeq n$ for large multiplicities. The transverse mass spectra exhibit an exponential decay in the transverse mass $m_{\perp n}$ with a slope parameter given by Eq. (48), i.e., which is determined by the value of the saddle point β , the rapidity y_n of the particle considered, and the parameter a . The slope parameter depends on the mass of the considered particle only through the position β of the saddle point of the phase-space integral. However, this dependence is very weak, because the position of the saddle point is largely decided by the values of the total multiplicity n and the total available energy $\sqrt{s} \gg m_n$. Quantitatively, the slope parameter varies by less than 0.1 % in the range of particle masses 0 – 2 GeV. As a consequence, in this simple phase-space model the transverse mass spectra of all particle species have the same slope.

In Fig. 3 we demonstrate the exponential decay of the transverse mass spectra by showing π^- transverse mass spectra for different rapidities, computed from Eq. (47) with $a = 0$ and using the particle multiplicities of Table II to compute the phase-space integrals. One observes that the slope parameter increases with increasing rapidity, as is obvious from Eq. (48).

The case where $a = 0$ and all particles are massless deserves a special treatment. If all particles have the same mass, then the mean multiplicity of the n th particle is simply the total multiplicity, $\langle n_n \rangle \equiv n$, and we obtain for the transverse mass spectrum (omitting the index n) [16]

$$\frac{1}{m_{\perp}} \frac{d^2 n}{dm_{\perp} dy} = \pi n \frac{I_{n-1}(s')}{I_n(s)} = \frac{2n(n-1)(n-2)}{s} \left(1 - \frac{2m_{\perp} \cosh y}{\sqrt{s}}\right)^{n-3} , \quad (49)$$

where we have used Eqs. (37) and (43). Using the saddle-point condition $\beta \equiv 2n/\sqrt{s}$, cf. Eq. (34), and $(1-x/n)^n \simeq e^{-x}$ (valid for large n), we obtain

$$\frac{1}{m_{\perp}} \frac{d^2 n}{dm_{\perp} dy} \simeq n \frac{\beta^2}{2} e^{-\beta m_{\perp} \cosh y} , \quad (50)$$

where we have dropped subleading terms of order $O(1/n)$. One observes that the transverse mass spectrum is exponentially decreasing as a function of the particle energy $E \equiv m_{\perp} \cosh y$. From Eq. (34) we see that the inverse slope parameter $1/\beta$ corresponds to half of the available energy per particle. We note that the result (50) could have also been obtained from Eqs. (47) and (48). To see this, employ $a = 0$ and Eq. (37) to show that $1/T^* = \beta$. Note that the apparent “temperature” T^* is half the energy per particle, $T^* = \frac{1}{2}\sqrt{s}/n$ [16, 27]. This is in contrast to the temperature T for an ultrarelativistic gas in thermal equilibrium, which appears instead of T^* in the transverse mass spectrum, see Eq. (55) below, and which is one third of the thermal energy per particle, $T = \frac{1}{3}E/n$. Thus, if we compare transverse mass spectra for the phase-space model and the thermal model at the same total energy, $\sqrt{s} = E$,

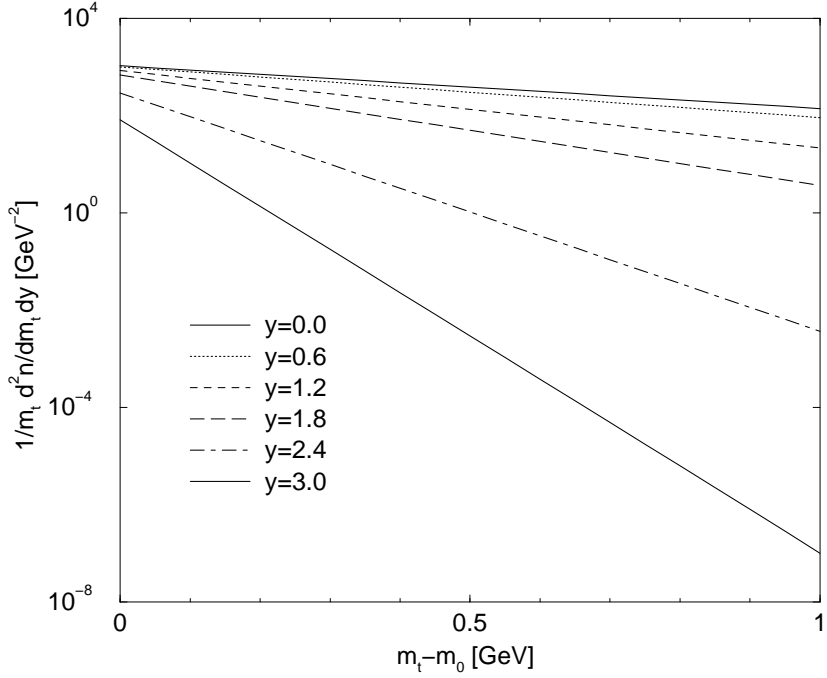


FIG. 3: Transverse mass spectra for π^- -mesons in Pb+Pb-reactions at 158 AGeV.

the apparent temperature is a factor $3/2$ times the thermal temperature, $T^* = \frac{3}{2} T$. The inverse slope parameter T^* of the transverse mass spectra should thus not be interpreted as the temperature in thermodynamical equilibrium.

Integrating either the exact result (49) or the approximate result (50) for the transverse mass spectrum of massless particles over m_\perp , we obtain the rapidity spectrum

$$\frac{dn}{dy} = \frac{n}{2 \cosh^2 y}. \quad (51)$$

The half width Δy of the rapidity spectrum for massless particles is independent of the particle number and the total energy \sqrt{s} of the reaction, $\Delta y = \ln(1 + \sqrt{2}) \simeq 0.8814$. A further integration gives

$$\int dy \frac{dn}{dy} = n \int \frac{dy}{2 \cosh^2 y} = n, \quad (52)$$

as expected.

C. The thermal model

We shall compare our transverse mass spectrum computed from the phase-space integral with those obtained in a thermal model. The latter are obtained from the Cooper-Frye formula [39]

$$E_n \frac{dn_n}{d^3 p_n} \equiv \frac{1}{m_{\perp n}} \frac{dn_n}{dm_{\perp n} dy_n} = \int_{\Sigma} d\sigma_{\nu} p_n^{\nu} g_n(x, p_n), \quad (53)$$

which counts the number of on-shell particles with three-momentum \mathbf{p}_n streaming through a space-time hypersurface Σ with normal vector $d\sigma_{\mu}$. Here, $g_n(x, p_n)$ is the single-particle on-shell momentum distribution function for the n th particle at space-time point x and Σ is the hypersurface where kinetic freeze-out of particles occurs. In general, this hypersurface could have a complicated shape in space-time. Here, we make the simplifying assumption that freeze-out occurs at fixed time in the center-of-momentum frame, such that $d\sigma_{\nu} = (d^3 x, \mathbf{0})$. Provided that $g_n(x, p_n)$ does not change over the freeze-out hypersurface, the integration over $d\sigma_{\nu}$ then simply yields a factor V , the total volume of the system. We also take the particles to be distributed according to the appropriate quantum statistical distribution function in thermal equilibrium, $g_n(x, p_n) = d_n / (2\pi)^3 (e^{(E_n - \mu_n)/T} \pm 1)^{-1}$, where d_n is the degeneracy and μ_n the

chemical potential. The upper sign holds for fermions and the lower for bosons. The invariant momentum spectrum (53) reduces to

$$\frac{1}{m_{\perp n}} \frac{dn_n}{dm_{\perp n} dy_n} = \frac{d_n V}{(2\pi)^3} \frac{m_{\perp n} \cosh y_n}{e^{(m_{\perp n} \cosh y_n - \mu_n)/T} \pm 1}. \quad (54)$$

For particle energies $E_n = m_{\perp n} \cosh y_n \gg T, \mu_n$, this becomes the classical Boltzmann distribution,

$$\frac{1}{m_{\perp n}} \frac{dn_n}{dm_{\perp n} dy_n} \simeq \frac{d_n V e^{\mu_n/T}}{(2\pi)^3} m_{\perp n} \cosh y_n e^{-m_{\perp n} \cosh y_n/T}. \quad (55)$$

Note that this thermal distribution is not an exponential in the particle energy $E_n = m_{\perp n} \cosh y_n$ because of the prefactor $m_{\perp n} \cosh y_n$ which introduces logarithmic corrections to the pure exponential decay.

In this work, we do not attempt to fit the temperature, the volume, and the chemical potential to reproduce the particle multiplicities. There is a vast amount of literature regarding such fits, see e.g. [6–8]. Our goal is to compare the invariant phase space available to the system at a given energy to the corresponding thermodynamic phase space. To this end, we note that all hadrons except pions are sufficiently heavy so that the Boltzmann approximation (55) for the particle spectra is applicable. In this case, the chemical potential only enters the overall normalization of the invariant momentum spectrum, but does not change its shape. For pions, on the other hand, the chemical potential is in general quite small [6–8]. It is therefore justified to use the following ansatz for the particle spectra

$$\frac{1}{m_{\perp n}} \frac{dn_n}{dm_{\perp n} dy_n} = c_n \frac{m_{\perp n} \cosh y_n}{e^{m_{\perp n} \cosh y_n/T} \pm 1}, \quad (56)$$

where c_n contains the information about the volume of the system, the degeneracy, and the chemical potential and is determined from the multiplicity of the n th particle,

$$\langle n_n \rangle = c_n \int d^3 p_n \frac{1}{e^{E_n/T} \pm 1}. \quad (57)$$

The rapidity spectrum dn_n/dy_n is obtained from Eq. (56) by integrating over $m_{\perp n}$.

In order to compute the invariant momentum spectrum (56), we still need to fix the temperature. We choose it such that the total thermal energy E is equal to the center-of-momentum energy \sqrt{s} available for particle production,

$$\sqrt{s} \equiv E = \sum_r \int d^3 p_r E_r \frac{1}{m_{\perp r}} \frac{dn_r}{dm_{\perp r} dy_r} = \sum_r c_r \int d^3 p_r \frac{E_r}{\exp(E_r/T) \pm 1}, \quad (58)$$

where r labels the particle species.

IV. COMPARISON WITH EXPERIMENTAL DATA

In this section, we compute transverse mass and rapidity spectra from both the phase space as well as the thermal model and compare them to the experimental data.

A. Completing particle multiplicities in central Pb+Pb collisions at 158 AGeV

The calculation of the phase-space integral requires knowledge of the multiplicities of the various particle species, their masses, and the total energy of the reaction. Since the NA49 experiment does not measure all particle species produced in a nuclear collision, the multiplicity data [20–25] must be completed by using symmetry considerations, electric charge, baryon number and strangeness conservation, as well as empirical rules.

We assume that the n particles in the final state are solely produced by strong interactions. Therefore, the multiplicities measured in the experiment have to be corrected for weak decays. This has already been done in the data of the NA49 collaboration [20]. We show the measured multiplicities for pions, kaons, Λ 's, Ξ 's, and Ω 's in Table I.

Based on Table I, we now reconstruct the multiplicities for particle species not directly measured by NA49.

Hadron	m_r [GeV]	$\langle n_r \rangle$	Hadron	m_r [GeV]	$\langle n_r \rangle$
π^+	0.1396	619.0	$\bar{\Lambda}$	1.1157	4.64
π^-	0.1396	639.0	Ξ^-	1.3213	4.45
K^+	0.4937	103.0	Ξ^+	1.3213	0.83
K^-	0.4937	51.9	Ω	1.6725	0.62
K_S^0	0.4977	81.0	$\bar{\Omega}$	1.6725	0.20
Λ	1.1157	53.0			

TABLE I: Multiplicities of different particle species measured by the NA49 collaboration [20] in Pb+Pb collisions at 158 AGeV and corrected for weak decays.

- π^0 : Due to (approximate) isospin symmetry in the reaction, we take

$$\langle \pi^0 \rangle = \frac{\langle \pi^+ \rangle + \langle \pi^- \rangle}{2}. \quad (59)$$

- K^0, \bar{K}^0 : We assume that $\langle K_S^0 \rangle = \langle K_L^0 \rangle$ and $\langle K^0 \rangle = \langle \bar{K}^0 \rangle$. Since $\langle K^0 \rangle + \langle \bar{K}^0 \rangle = \langle K_S^0 \rangle + \langle K_L^0 \rangle$, we have

$$\langle K^0 \rangle = \langle \bar{K}^0 \rangle = \langle K_S^0 \rangle. \quad (60)$$

- $\Lambda, \Sigma^+, \Sigma^0, \Sigma^-$: An empirical rule found by Wroblewski [40, 41] states that

$$\langle \Sigma^+ \rangle + \langle \Sigma^- \rangle = 0.6 [\langle \Lambda \rangle + \langle \Sigma^0 \rangle]. \quad (61)$$

Here, $\langle \Lambda \rangle + \langle \Sigma^0 \rangle$ corresponds to the number of *measured* Λ 's as given in Table I. Note that the measured Λ multiplicity is not the *true* multiplicity, $\langle \Lambda \rangle$, because the Σ^0 decays to 100% into a Λ . One therefore has to reduce the measured Λ multiplicity by that of the Σ 's. Equation (61) yields the combined multiplicity of Σ^+ and Σ^- directly from the measured data. Due to isospin symmetry, we may assume that

$$\langle \Sigma^0 \rangle = \frac{\langle \Sigma^+ \rangle + \langle \Sigma^- \rangle}{2}. \quad (62)$$

Now the multiplicities of $\Sigma^+ + \Sigma^-$ and Σ^0 are known. Combining Eqs. (61) and (62), we can solve for $\langle \Lambda \rangle$,

$$\langle \Lambda \rangle = \frac{7}{3} \langle \Sigma^0 \rangle = \frac{7}{6} [\langle \Sigma^+ \rangle + \langle \Sigma^- \rangle] = 0.7 [\langle \Lambda \rangle + \langle \Sigma^0 \rangle]. \quad (63)$$

The multiplicities for the corresponding antiparticles are obtained in the same way.

- $\Xi^0, \bar{\Xi}^0$: Due to isospin symmetry we have

$$\langle \Xi^0 \rangle = \langle \Xi^- \rangle, \quad \langle \bar{\Xi}^0 \rangle = \langle \Xi^+ \rangle. \quad (64)$$

- Nucleons: The net number of protons and neutrons follows from baryon number conservation,

$$\begin{aligned} \langle p \rangle - \langle \bar{p} \rangle + \langle n \rangle - \langle \bar{n} \rangle \\ = N_w - [\langle \Lambda \rangle - \langle \bar{\Lambda} \rangle + \langle \Sigma^+ + \Sigma^- \rangle - \langle \bar{\Sigma}^+ + \bar{\Sigma}^- \rangle + \langle \Xi^0 \rangle - \langle \bar{\Xi}^0 \rangle + \langle \Xi^- \rangle - \langle \Xi^+ \rangle + \langle \Omega^- \rangle - \langle \Omega^+ \rangle] \\ = 276.96, \end{aligned} \quad (65)$$

where we have used the number of wounded nucleons N_w and the previously determined multiplicities. Assuming isospin symmetry,

$$\langle p \rangle = \langle n \rangle, \quad \langle \bar{p} \rangle = \langle \bar{n} \rangle, \quad (66)$$

we get $\langle p \rangle - \langle \bar{p} \rangle = \langle n \rangle - \langle \bar{n} \rangle = 138.48$. In order to obtain the individual multiplicities, we assume that the production of strange antiquarks relative to strange quarks is suppressed as compared to the production of nonstrange antiquarks relative to nonstrange quarks by a factor $D \equiv \frac{\langle \bar{s} \rangle \langle q \rangle}{\langle s \rangle \langle \bar{q} \rangle}$ [42, 43]. This results in

$$\frac{\langle \bar{p} \rangle}{\langle p \rangle} = D^{-1} \frac{\langle \bar{\Lambda} \rangle}{\langle \Lambda \rangle} = D^{-2} \frac{\langle \Xi^+ \rangle}{\langle \Xi^- \rangle} = D^{-3} \frac{\langle \Omega^+ \rangle}{\langle \Omega^- \rangle}. \quad (67)$$

D can be obtained from the measured multiplicities. We take the average value of $\frac{\langle \Xi^+ \rangle}{\langle \Xi^- \rangle} / \frac{\langle \bar{\Lambda} \rangle}{\langle \Lambda \rangle}$ and $\frac{\langle \Omega^+ \rangle}{\langle \Omega^- \rangle} / \frac{\langle \Xi^+ \rangle}{\langle \Xi^- \rangle}$, respectively. This yields $D = 1.93$. The antiproton-to-proton ratio is then $\frac{\langle \bar{p} \rangle}{\langle p \rangle} = 0.0454$.

Hadron	m_r [GeV]	$\langle n_r \rangle$	Hadron	m_r [GeV]	$\langle n_r \rangle$
π^+	0.1396	619	$\bar{\Sigma}^+ + \bar{\Sigma}^-$	1.1934	3
π^-	0.1396	639	Ξ^-	1.3213	4
π^0	0.1350	629	Ξ^+	1.3213	1
K^+	0.4937	103	Ξ^0	1.3148	4
K^-	0.4937	52	$\bar{\Xi}^0$	1.3148	1
$K^0 + \bar{K}^0$	0.4977	162	$\Omega + \bar{\Omega}$	1.6725	1
Λ	1.1157	37	p	0.9383	145
$\bar{\Lambda}$	1.1157	3	\bar{p}	0.9383	7
$\Sigma^+ + \Sigma^-$	1.1934	32	n	0.9396	145
Σ^0	1.1926	16	\bar{n}	0.9396	7
$\bar{\Sigma}^0$	1.1926	1			

TABLE II: Completed list of multiplicities.

The completed multiplicities are summarized in Table II. The average number of the secondaries thus obtained is 2611. Note that we do not attempt to reconstruct resonances decaying strongly into pions and nucleons, such as the ρ and the Δ . In order to determine the corresponding multiplicities one would require additional assumptions, e.g. thermodynamical equilibrium between various particle species. As we aim to present an approach that is complementary to the thermal model, we refrain from doing so. Moreover, one would then have to treat the decay of these reconstructed resonances separately in order to compare with the measured spectra which already contain decay products. We leave this for a future improvement of our approach and, in this work, do not make a distinction between direct particle production and subsequent resonance decay.

B. Transverse mass and rapidity spectra from phase space, $a = 0$

In this section, we compute pion and kaon spectra from the phase-space model with $a = 0$ and compare them to experimental NA49 data from the 5% most central Pb+Pb collisions at 158 AGeV.

Figure 4 shows transverse mass spectra for π^- , K^+ , and K^- mesons, calculated from the phase-space model as well as from a thermal model, together with the measured data. We observe that the phase-space model and the thermal model give quite similar results. The agreement becomes better for larger particle mass. This is not surprising, since the nonrelativistic limit of relativistic invariant phase space, $\int d^3\mathbf{p}_i/E_i \rightarrow (1/m_i) \int d^3\mathbf{p}_i$, is identical to the phase space in the thermal model.

However, both models disagree with the data. The slope is too small, i.e., the inverse slope parameter is too large. In the phase-space model, $T_\pi^* = 0.4935$ GeV and $T_K^* = 0.4934$ GeV. In the thermal model, the temperature parameter extracted from the energy constraint (58) is $T = 0.374$ GeV for both pions and kaons. Note that the inverse slope parameter T^* is larger than the temperature T , $T^*/T \simeq 1.32$. In the ultrarelativistic limit, $T^*/T = \frac{3}{2}$, cf. discussion above. In the nonrelativistic limit, i.e., for $m_i \gg T$, $T^*/T \rightarrow 1$, since then invariant phase space becomes identical to thermodynamic phase space. Pions and kaons are neither ultrarelativistic nor nonrelativistic, which explains the value $T^*/T \simeq 1.32$, i.e., between 1 and $3/2$. In the range of m_\perp values shown in Fig. 4, both spectra appear to have a similar slope, but at larger m_\perp , the thermal model spectrum decays faster than the one calculated from the phase-space model, as it should, since its inverse slope parameter T is smaller than T^* by $\sim 30\%$.

Let us now consider the rapidity spectra. Figure 5 shows the measured spectrum of π^- mesons in comparison to the phase-space model and the thermal model. Phase-space and thermal model give almost identical results. However, the calculated rapidity spectra are much narrower than the measured one. Similar results hold for K^+ mesons, see Fig. 6.

How sensitive are the calculated spectra to variations in the total multiplicity? To answer this question, we performed two tests. First, we added 200 massless particles and, alternatively, 200 particles with mass 1 GeV, to the set of 2611 particles. For a given, sufficiently large \sqrt{s} , this increases the derivative of $\ln I_{n-1}$ with respect to \sqrt{s} . Then, according to Eq. (48), the slope parameter $1/T^*$ of the transverse mass spectra increases. This increase is independent of rapidity and the mass of the considered particle species. It amounts to 7.5% when adding massless particles and to 14% when adding particles with mass 1 GeV. The difference between adding massless and massive particles can be explained from Fig. 1: the increase of $\ln I_{n-1}$ with \sqrt{s} is smaller for massless particles, thus, according

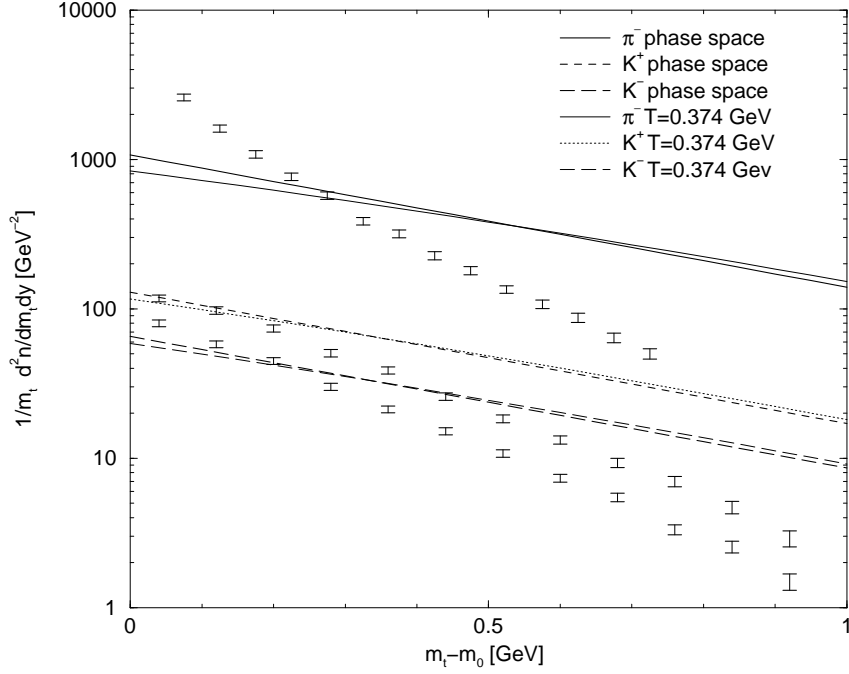


FIG. 4: Transverse mass spectra for π^- , K^+ , and K^- calculated from the phase-space model with $a = 0$, as well as from a thermal model. The pion data is taken in the range $0 < y < 0.2$, and the kaon data for $|y| < 0.1$. Experimental data is shown by the symbols. Here, as in the following figures, error bars include statistical errors (as given by NA49) and a systematical error of 5%.

to Eq. (48), the increase of the slope parameter $1/T^*$ when adding particles is also smaller. An uncertainty of 200 in the total multiplicity can therefore not explain the deviation between the measured and the calculated transverse mass spectra for pions and kaons.

Second, we changed the total multiplicity by $k \times 260$ particles, where $k = -1, 1, 2$, preserving the ratio between the multiplicities of different particle species. Figure 7 shows the transverse mass spectra. The inverse slope decreases with increasing multiplicity, but even 560 additional particles are not sufficient to reproduce the measured spectra. In Fig. 8 we show the corresponding rapidity spectra for $k = -1, 0, 1$ together with the experimental data in a logarithmic plot. The distributions become narrower with increasing multiplicity. Thus, while the slope values of the transverse mass spectra approach the data for increasing multiplicity, the rapidity distributions deviate more strongly. It is therefore not possible to simultaneously reproduce transverse mass spectra and rapidity spectra simply by varying the total multiplicity.

C. Transverse mass and rapidity spectra from phase space, $a \neq 0$

We have seen that the transverse mass spectra calculated from the phase-space model with $a = 0$ do not agree with the experimental data: their inverse slope parameter is too large. Similarly, the calculated rapidity spectra are too narrow. This indicates a substantial remnant of the initial longitudinal motion of target and projectile, which still dominates the phase space. Or in other words, complete isotropization has not occurred.

The introduction of the factors $f_i(\mathbf{p}_{\perp i})$, cf. Eq. (6), with $a > 0$, allows to suppress the transverse in favor of the longitudinal phase space. The parameter a regulates the strength of the suppression of transverse momenta and has to be extracted from the data. There are in principle two possibilities: (1) a is adjusted to reproduce the transverse mass spectra, or (2) a is adjusted to reproduce the rapidity spectra.

In Figs. 9 and 10 we show the transverse mass and rapidity spectrum for π^- mesons, calculated from the phase-space model in comparison with experimental data. Choosing the value $a = (0.2 \text{ GeV})^{-1}$, we can quite well reproduce the transverse mass spectrum. However, the rapidity spectrum is then wider than the data, which indicates that the suppression of transverse phase space is slightly too large. Note that, at small transverse masses, the pion data lie above the calculated curve. This is quite naturally explained by the fact that our simple phase-space model does not account for the distortion of phase space due to resonance decays. Such resonance decays are expected to populate

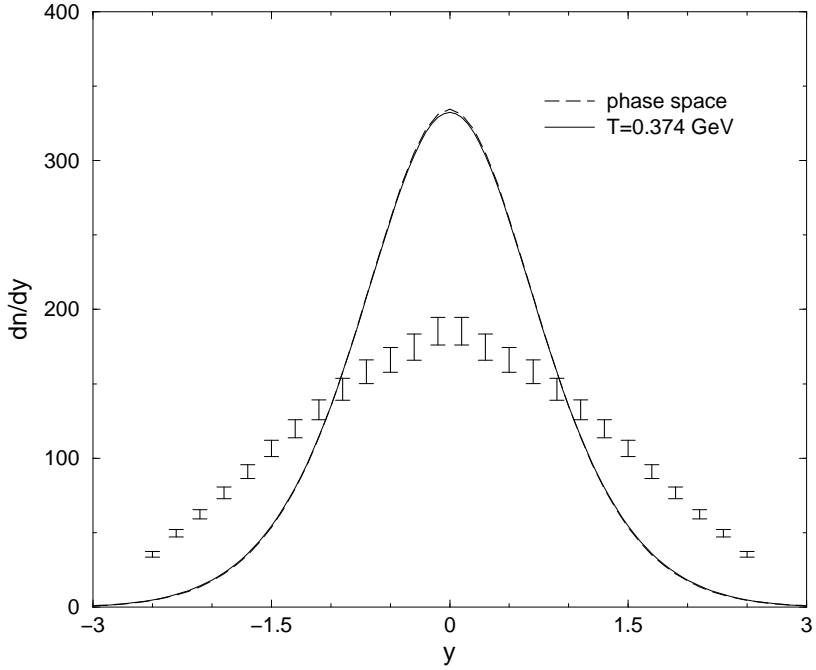


FIG. 5: Rapidity spectra for π^- mesons, experimental data are shown by symbols, results from the phase-space model by the dashed line and from the thermal model by the solid line.

meson	$T_{\text{exp}}^* [\text{GeV}]$	$a^{-1} [\text{GeV}^{-1}], m_{\perp}\text{-fit}$	$a^{-1} [\text{GeV}^{-1}], y\text{-fit}$
π^-	0.180	0.200	0.325
K^+	0.232	0.272	0.213
K^-	0.226	0.263	0.315

TABLE III: Optimal values for the damping parameter a .

mainly the low-transverse mass region where we observe the difference between the data and the calculation [15].

Figures 11 and 12 show the transverse mass and rapidity spectrum, now for a value $a = (0.325 \text{ GeV})^{-1}$ which is adjusted to reproduce the rapidity spectrum. In this case, the calculated transverse mass spectrum differs from the data in that the inverse slope comes out too large. Transverse phase space is not sufficiently suppressed in this case. Comparing the set of Figs. 9, 10 with the set of Figs. 11, 12 suggests that there is a value for a between $(0.2 \text{ GeV})^{-1}$ and $(0.325 \text{ GeV})^{-1}$, for which a simultaneous fit of *both* transverse mass and rapidity spectrum, albeit of worse quality than the individual fits shown in Fig. 9 and Fig. 12, could be possible. Before returning to this question, we summarize in Table III the optimal fit values for the parameter a for π^- , K^+ , and K^- mesons. In the first column, we quote the experimentally measured value of the slope parameter of the transverse mass spectrum, T_{exp}^* . In the second column we show the a -values optimized to fit the transverse mass spectra, and in the last column those optimized to fit the rapidity spectra. Note that, for the kaon spectra, the two a values thus obtained are quite close to each other. Indeed, either a fit to the transverse mass spectrum or to the rapidity spectrum will also yield a reasonable description of the respective other spectrum.

We now ask the question whether there is a single value for a which gives a reasonable description of both the transverse mass and the rapidity spectrum, and not only for pions but also for kaons. This is indeed the case, as shown in Figs. 13, 14, and 15, for $a = (0.256 \text{ GeV})^{-1}$. It is quite remarkable that, for a given set of particle multiplicities, a single parameter that accounts for longitudinal phase-space dominance is sufficient to yield a simultaneous fit of the transverse mass and rapidity spectra for *both* pions and kaons. The observed deviations can be quite easily explained. In the case of the pions, resonance (e.g. ρ and Δ) decays populate the region of small transverse momenta and thus lead to an enhancement of the measured as compared to the calculated transverse mass spectrum. For the kaons, one observes that the measured transverse mass spectra exhibit a convex curvature indicative for collective flow of

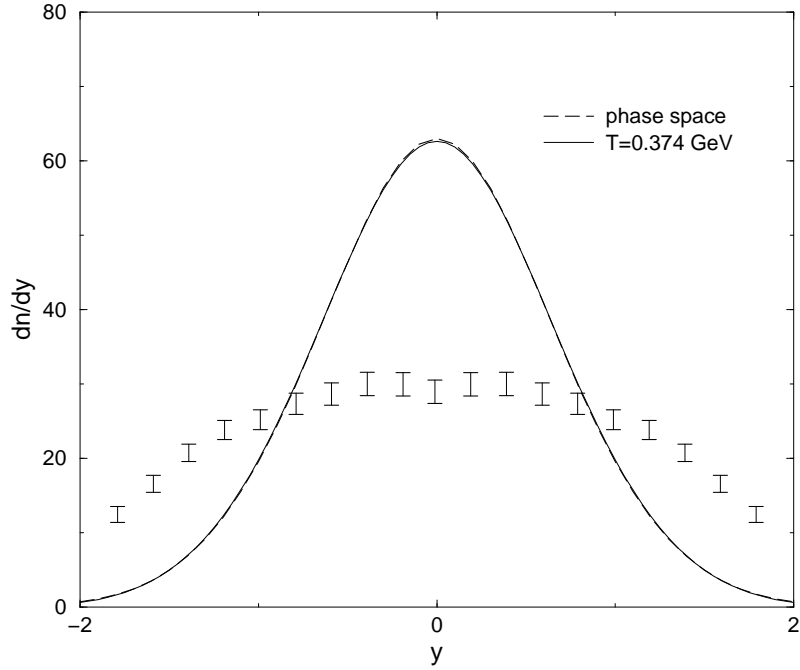


FIG. 6: The same as in Fig. 5 for K^+ mesons.

matter. This is a nontrivial dynamical effect not contained in our simple phase-space approach. Collective flow is more prominent for heavier particle species not considered here and will lead to similar deviations from the spectra calculated within our simple phase-space approach. Nevertheless, we expect that the quality of the fit can be further improved by introducing separate parameters a_r for each particle species r . This, however, as well as a more refined treatment of resonance decays, is beyond the scope of the present work where we want to keep the treatment as simple as possible.

V. SUMMARY AND OUTLOOK

We have studied particle production in nuclear collisions within a phase-space model. Assuming a simple form for the matrix element that describes the production of n secondary particles, we have computed the phase-space integral within a statistical approach based on the Laplace transformation and the saddle-point method. Single-inclusive invariant momentum spectra can be then computed from the ratio of the phase-space integrals for $n-1$ and n particles, respectively.

We have applied this phase-space approach to multiparticle production to data for Pb+Pb collisions at 158 AGeV taken by the NA49 collaboration. In order to compute the phase-space integral, we require (a) the total available energy which is determined from the beam energy and the number of wounded nucleons (in our case, $\sqrt{s} = 3131.3$ GeV) and (b) the multiplicities and the masses of the various particle species produced in the reaction. However, the NA49 experiment does not measure all species of strongly interacting particles. We reconstructed the multiplicities of the most important missing particle species using symmetry considerations, conservation laws, a simple quark model and an empirical rule. In this way we obtained 2611 secondary particles. By changing this value by - 10% and +20%, respectively, we tested the sensitivity of our results to the reconstruction procedure and found that this does not affect our conclusions.

From the phase-space integral we then computed transverse mass and rapidity spectra for π^- , K^+ , and K^- mesons and compared them with the measured spectra. Our simple model predicts transverse mass spectra of exponential shape, with an inverse slope parameter that is (almost) independent of the particle mass.

We also computed transverse mass and rapidity spectra assuming the system to be in thermal equilibrium at a temperature which is determined from the total available energy $\sqrt{s} = 3131.3$ GeV. In the thermal model, transverse mass spectra are not pure exponentials, but are of slightly convex shape. At midrapidity, the inverse slope parameter of the transverse mass spectra is identical to the temperature, T , and smaller than the inverse slope parameter, T^* ,

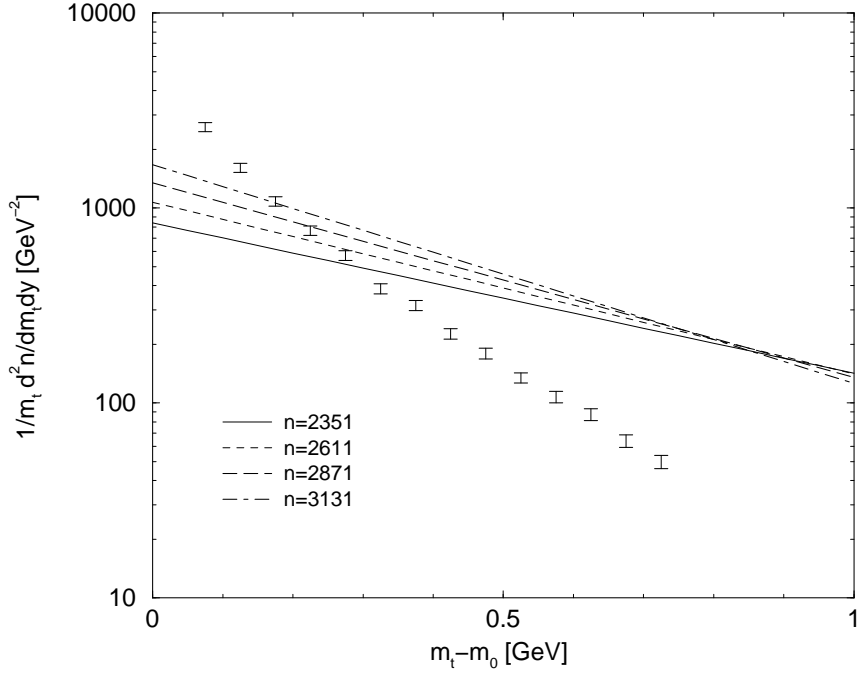


FIG. 7: Transverse mass spectrum for π^- mesons for different total multiplicities n .

arising in the phase-space model. This difference can be traced to the different definitions of phase space in the two models, invariant phase space $d^3\mathbf{p}_i/E_i$ for the phase-space model, and non-invariant phase space $d^3\mathbf{p}_i$ for the thermal model. For ultrarelativistic particles, the difference in the slope parameters can be computed analytically, $T^*/T = 3/2$. Due to the convex shape of the transverse mass spectra in the thermal model, in the range of transverse masses $0 \leq m_\perp - m \leq 1$ GeV, the transverse mass spectra in both models are surprisingly similar. The difference in the slope parameters becomes visible only at larger transverse masses. The rapidity spectra of the thermal and the phase-space model are also very similar.

If we assume a constant, i.e., isotropic matrix element for multiparticle production, the transverse mass and rapidity spectra calculated from the phase-space model deviate substantially from the experimentally measured spectra. The same holds for the thermal model. This deviation is due to the fact that there is still a remnant of the initial, longitudinal motion of the nuclei such that the phase space is not isotropically populated in the final state.

There are two possibilities to obtain agreement between models and data. The first possibility is to retain the assumption of an isotropic phase-space distribution *locally* in coordinate space. One then employs a dynamical model for the evolution of matter, such as fluid dynamics, which gives rise to collective transverse as well as longitudinal flow of matter. For a given equation of state, one can then tune the initial as well as the freeze-out conditions in order to reproduce the data and thus account for longitudinal phase-space dominance.

In this paper, we pursue the second possibility. We relax the assumption of isotropic phase space and take longitudinal phase-space dominance into account by a simple ansatz for the matrix element which exponentially suppresses transverse momenta. This has the effect that the transverse mass spectra decrease faster and the rapidity spectra become wider. The amount of suppression is determined by a parameter a which is fitted to the experimental spectra. The best fits were obtained by choosing different parameters a for each type of particle (π^+ , K^+ , K^-) and fitting transverse mass spectra and rapidity spectra separately. Surprisingly, a rather good fit of transverse mass and rapidity spectra of all particles considered can also be obtained by a single value, $a = (0.256 \text{ GeV})^{-1}$. Note that this second approach does not require the assumption of thermal equilibrium. Observed deviations between calculated and measured spectra can be attributed to nontrivial dynamical phenomena, such as resonance decays and collective flow.

A possible extension of our present work is to compare our phase-space model with data for heavier particles, such as nucleons and hyperons. It is known that the transverse mass spectra of particles heavier than pions and kaons have a substantially larger inverse slope parameter (but essentially of similar magnitude for all of them). This is usually attributed to the collective radial flow of matter [44]. In order to incorporate this into our approach, we would have to introduce one additional parameter a for the heavier particle species. The other way to account for different slope

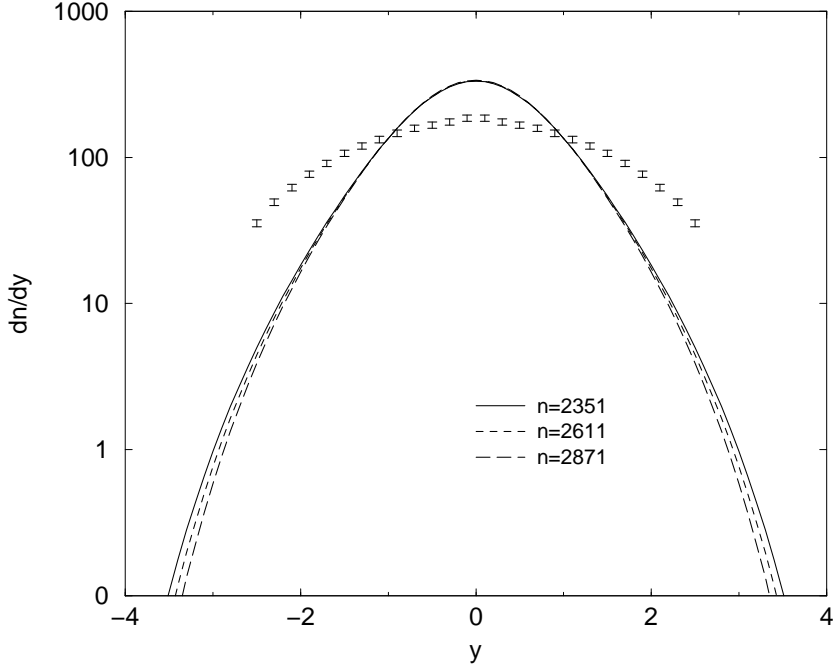


FIG. 8: Rapidity spectrum for π^- mesons for different total multiplicities n .

parameters for the various particle species would be to use a more physical ansatz for, or even a detailed calculation of, the matrix element $T(\mathbf{p}_i)$ [17]. Another possible extension is to incorporate the distortion of the phase-space of light particles, such as pions, by the decay of heavier resonances [13].

Acknowledgment

We thank A. Andronic, F. Becattini, M. Bleicher, A. Dumitru, C. Greiner, M. Gyulassy, K. Kajantie, J. Knoll, A. Kostyuk, J. Reinhardt, J. Schaffner-Bielich, I. Shovkovy, M. Strikman, Q. Wang, and G. Wilk for comments and discussions. We thank in particular M. Ga  dzicki for valuable discussions concerning the reconstruction of the multiplicities of particles in the experiment and for providing us with the multiplicities given in Table I. We also thank J. Stachel and P. Braun-Munzinger for providing us with a numerical routine for the saddle-point method.

[1] see, for instance, proc. of the 17th int. conf. on ultra-relativistic nucleus-nucleus collisions “Quark Matter 2004”, Oakland, USA, Jan. 1117, 2004 (eds. H.G. Ritter, X.N. Wang), *J. Phys. G*30 (2004) 633.

[2] for a review see, for instance, E. Laermann and O. Philipsen, *Ann. Rev. Nucl. Part. Sci.* 53 (2003) 163.

[3] P. Huovinen in *Quark-gluon plasma* (eds. R.C. Hwa, X.N. Wang, World Scientific, Singapore, 2004) 600.

[4] T.D. Lee, *Nucl. Phys. A*750 (2005) 1; M. Gyulassy and L. McLerran, *ibid.* 30; E. Shuryak, *ibid.* 64.

[5] P.F. Kolb and U.W. Heinz in *Quark-gluon plasma* (eds. R.C. Hwa, X.N. Wang, World Scientific, Singapore, 2004) 634.

[6] P. Braun-Munzinger, K. Redlich, and J. Stachel in *Quark-gluon plasma* (eds. R.C. Hwa, X.N. Wang, World Scientific, Singapore, 2004) 491.

[7] F. Becattini, M. Ga  dzicki, A. Keranen, J. Manninen, R. Stock, *Phys. Rev. C*69 (2004) 024905.

[8] S. Wheaton and J. Cleymans, [hep-ph/0407174](#).

[9] T. Hirano and K. Tsuda, *Phys. Rev. C*66 (2002) 054905.

[10] M. Gyulassy and T. Hirano, [nucl-th/0506049](#).

[11] K.J. Eskola, H. Niemi, P.V. Ruuskanen, and S.S. Rasanen, *Nucl. Phys. A*715 (2003) 561c.

[12] R. Hagedorn, *Relativistic Kinematics* (W.A. Benjamin, 1964).

[13] E. Byckling and K. Kajantie, *Particle Kinematics* (John Wiley & Sons, 1973).

[14] Y. Hama and M. Pl  mer, *Phys. Rev. D* 46 (1992) 160.

[15] J. Knoll, *Phys. Rev. C*20 (1979) 773; S. Bohrmann and J. Knoll, *Nucl. Phys. A*356 (1981) 498.

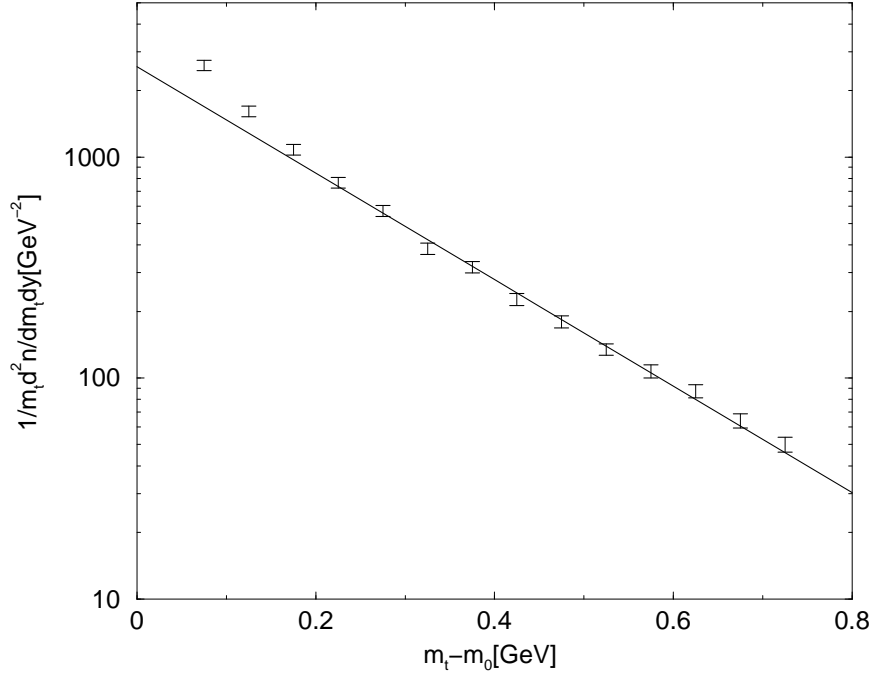


FIG. 9: Transverse mass spectrum for π^- mesons in the range $0 < y < 0.2$. The solid line shows the spectrum calculated from the phase-space model for $a = (0.2 \text{ GeV})^{-1}$.

- [16] D.H. Rischke, Nucl. Phys. A698 (2002) 153c.
- [17] J. Hormuzdiar, S.D.H. Hsu, and G. Mahlon, Int. J. Mod. Phys. E12 (2003) 649.
- [18] V. Koch, Nucl. Phys. A715 (2004) 108c.
- [19] F. Becattini, J. Phys. Conf. Ser. 5 (2005) 175.
- [20] Marek Ga  dzicki, private communication.
- [21] S.V. Afanasiev et al., Phys. Rev. C66 (2002) 054902.
- [22] A. Mischke et al., Nucl. Phys. A715 (2003) 453.
- [23] T. Anticic et al., Phys. Rev. Lett. 93 (2004) 022302.
- [24] S.V. Afanasiev et al., Phys. Lett. B538 (2002) 275.
- [25] C. Alt et al., Phys. Rev. Lett. 94 (2005) 192301.
- [26] K. Werner and J. Aichelin, Phys. Rev. C52 (1995) 1584.
- [27] B.L. Friman and J. Knoll, *Introduction to the physics of hot and dense hadronic matter*, lectures presented at GSI summer school 2000.
- [28] F. James, *Monte Carlo Phase Space*, CERN Report 68-15.
- [29] R. Kleiss and W.J. Stirling, Nucl. Phys. B385 (1992) 413.
- [30] F. Lur  at, P. Mazur, Nuov. Cim. XXXI (1964) 140.
- [31] A. Krzywicki, Nuov. Cim. XXXII (1967) 1067.
- [32] A. Krzywicki, J. Math. Phys. 6 (1965) 485.
- [33] A. Bialas and T. Ruijgrok, Nuov. Cim. XXXIX (1965) 1061.
- [34] K. Kajantie and V. Karim  ki, Comp. Phys. Commun. 2 (1971) 207.
- [35] K. Kajantie and V. Karim  ki, Ann. Acad. Sci. Fenn. Series A, VI. Physica, Vol. 395 (Helsinki, 1972)
- [36] A.J. Khinchin, *Mathematical Foundations of Statistical Mechanics* (Dover, New York, 1949).
- [37] I.S. Gradshteyn and I.M. Ryzhik, *Tables of Integrals, Sums, Series and Products*, Eq. (8.432.9) (Verlag Harri Deutsch, Frankfurt, 1981).
- [38] M. Abramowitz and I.A. Stegun, *Handbook of Mathematical Functions* (Dover, New York, 1965).
- [39] F. Cooper, G. Frye, and E. Schonberg, Phys. Rev. D11 (1975) 192.
- [40] A. Wroblewski, Acta Phys. Pol. B16 (1985) 379.
- [41] M. Gazdzicki and O. Hansen, Nucl. Phys. A528 (1991) 754.
- [42] J. Rafelski, Phys. Lett. B262 (1991) 333.
- [43] A. Bialas, Phys. Lett. B442 (1998) 449.
- [44] Nu Xu for the NA44 coll., Nucl. Phys. A610 (1996) 175c.

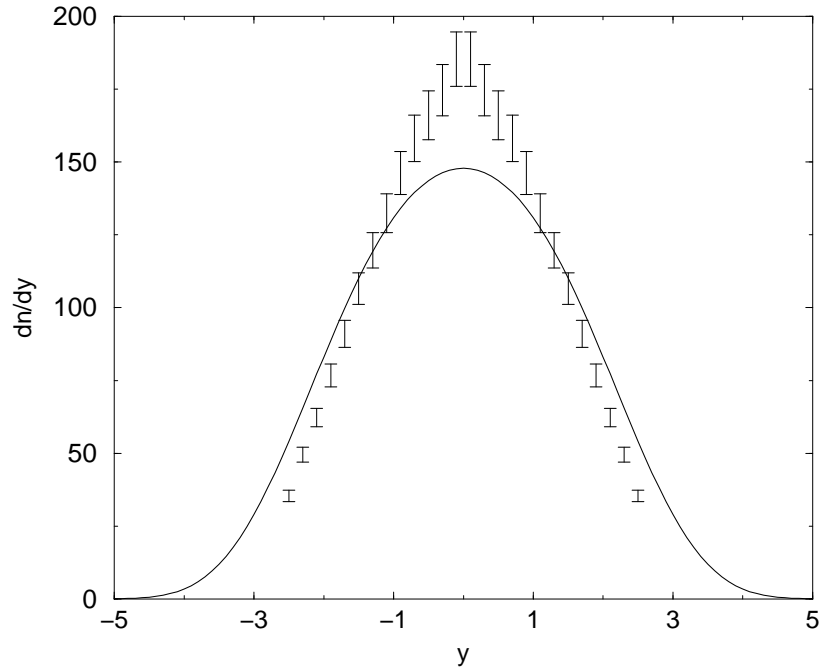


FIG. 10: The same as in Fig. 9, but for the π^- rapidity spectrum.

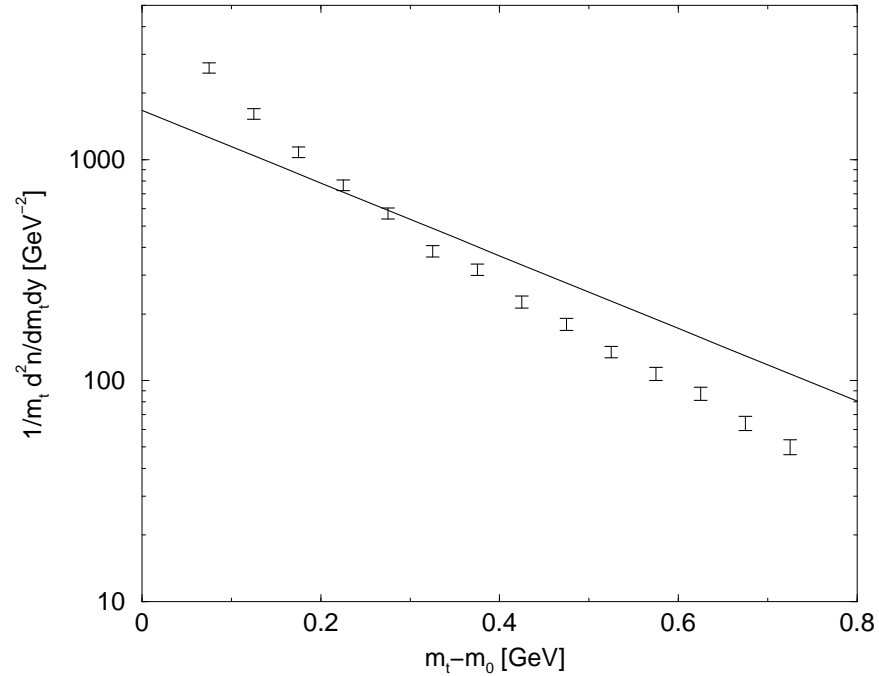


FIG. 11: The same as in Fig. 9, but with $a = (0.325 \text{ GeV})^{-1}$.

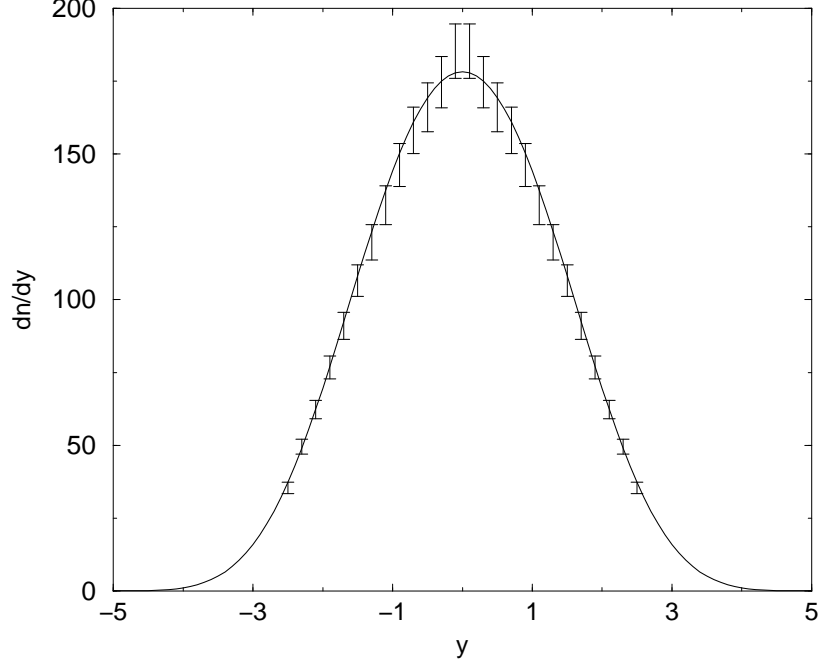


FIG. 12: The same as in Fig. 10, but with $a = (0.325 \text{ GeV})^{-1}$.

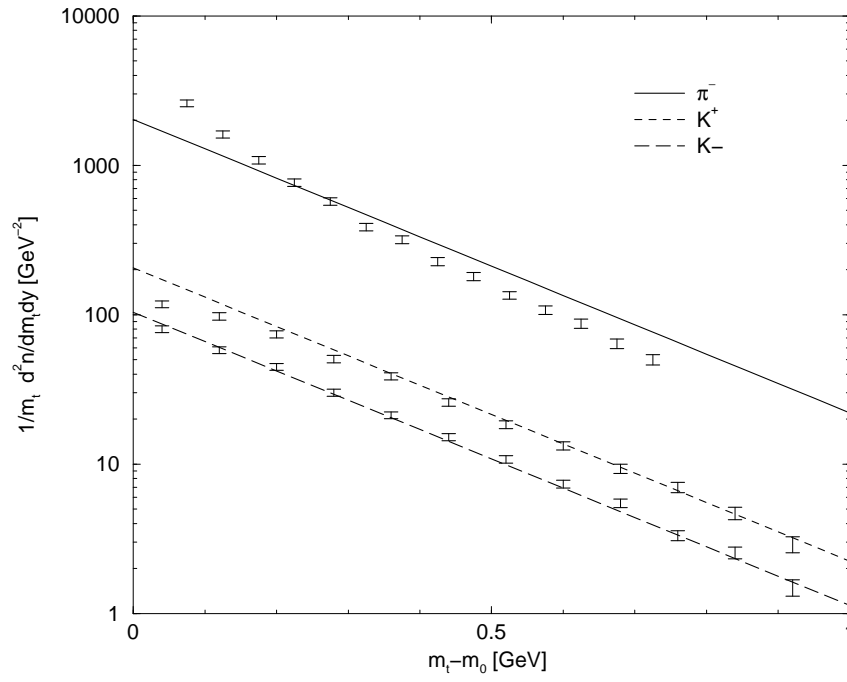


FIG. 13: Transverse mass spectra for π^- , K^+ , and K^- mesons. The solid lines show the spectra calculated from the phase-space model with $a = (0.256 \text{ GeV})^{-1}$.

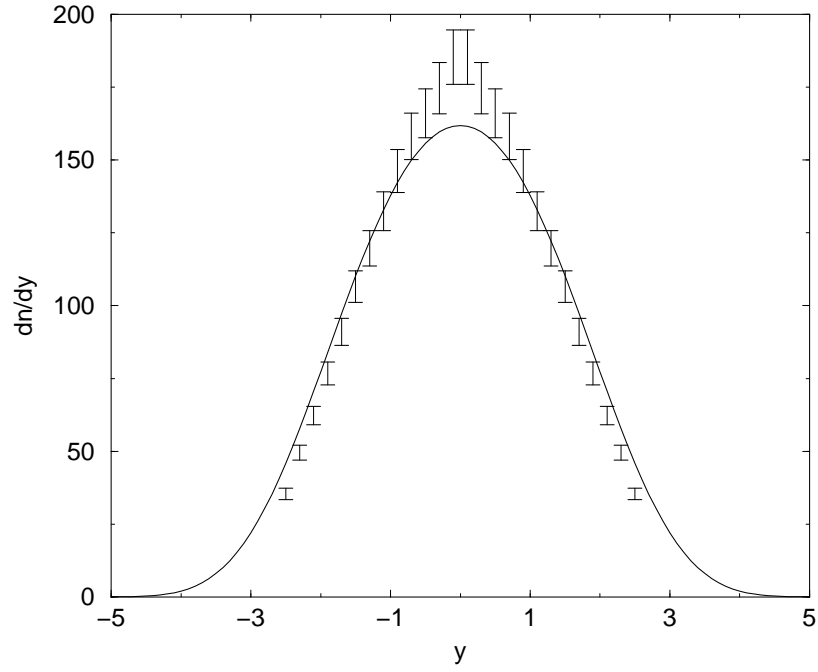


FIG. 14: Rapidity spectrum for π^- mesons. The solid line shows the spectrum calculated from the phase-space model with $a = (0.256 \text{ GeV})^{-1}$.

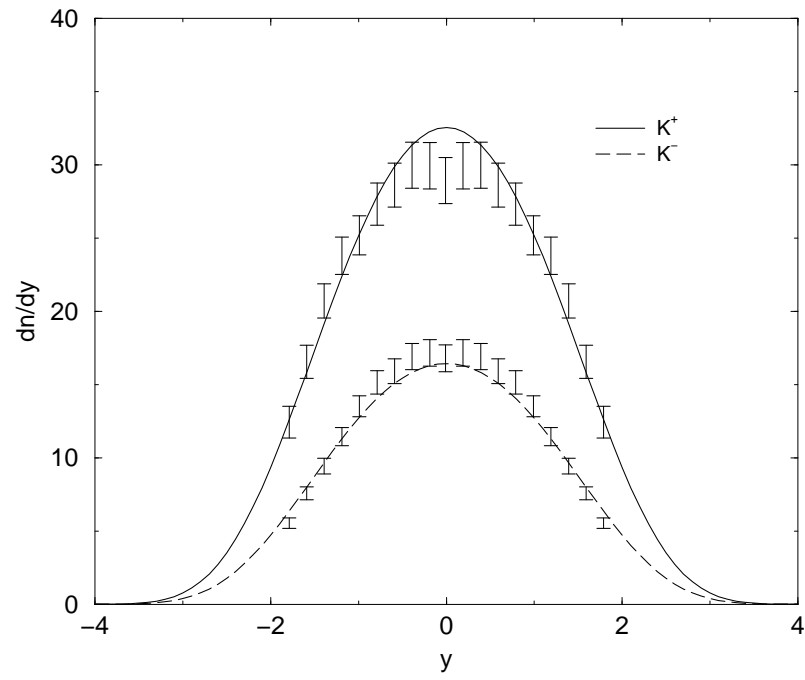


FIG. 15: The same as in Fig. 14, but for kaons.